Table 3 Initial tableau

			x_3	x_5
			1.0	1.34
0.92	x_1	0.84	−0.81	0.61
1.59	x_2	3.7	1.8*	−0.54
1.57	x_4	2.9		0.34
		11.2	1.12	−1.11

$x_1 - 0.81x_3 + 0.61x_5 = 0.84$
$x_2 + 1.8x_3 - 0.54x_5 = 3.7$
$x_4 + .34x_5 = 2.9$

Table 4 Final tableau

			x_2	x_5
			1.59	1.34
0.92	x_1	2.5	0.45	0.36
1.0	x_3	2.1	0.56	−0.3
1.57	x_4	2.9		0.34
		8.9	−0.62	−0.78

$x_1 + 0.45x_2 + 0.36x_5 = 2.5$
$x_3 + 0.56x_2 - 0.3x_5 = 2.1$
$x_4 + 0.34x_5 = 2.9$

matching the boundaries of the set, it would always run to the lowest point. This method is not limited to the case where there are two more variables than constraints. The approach is to specify one corner of the convex set by setting a sufficient number of the variables to zero. In the formulation of Vajda,[2] these are termed nonbasic variables. The number of these nonbasic variables equals the total number of variables minus the number of constraints. Having set the assumed nonbasic variables to zero, which specifies one corner of the convex set, the changes of the variable to be minimized (or maximized) are found along the edges of the convex set which lead from the corner of the set that was chosen. Then, a move is made along the edge where the change in the dependent variable is largest in the direction desired. This process is repeated until the changes in the dependent variable along the edges are all opposite to the direction desired. The corner at which this occurs is the optimum.

How this optimizing process can be accomplished through the use of tableaux is illustrated in Tables 3 and 4. For comparison, the problem is the same one that was solved graphically in Fig. 1. The independent variables that are to be set to zero for the first try are selected arbitrarily, and these are listed at the heads of the vertical columns. The other variables are placed next to the left end of the rows in the tableau. The equations of constraint are then solved to give each of the nonzero variables in terms of the zero variables (listed at the top of the columns). The pertinent equations are listed below the tableaux.

The body of each tableau is made up of a column of numbers just to the right of the column of nonzero variables (basic variables) that are adjacent to the extreme left of the tableau. These numbers are the constant terms in the equations listed below the tableau. The row of numbers just below the row of zero (nonbasic) variables that are listed at the top of the tableau are the coefficients c_j that give the effect on weight corresponding to the nonbasic variable listed above. Similar coefficients are listed to the left of the basic variables. Where coefficients or terms are zero they are not entered into the tableau. In the body of the tableau are numbers corresponding to a pair of variables consisting of one basic variable listed to the side and one nonbasic variable listed above. These numbers are the coefficients in the equations below the tableau defining the basic variables in terms of the nonbasic variables. By multiplying each number of the body of the tableau by the coefficient in its row just to the left of the basic variable, adding products, and subtracting the coefficient at the top of the column, the number at the bottom of the column is obtained. These are all checked, and if they are all negative the optimum has been found. If any are positive, the nonbasic variable at the top of the most positive value is moved over to be a basic variable in the next tableau. One of the basic variables is moved into the vacated place, and these two variables determine what is called the "pivot" in the initial tableau (noted by an asterisk). The pivot is located first by the column that has the largest positive number at the bottom. Secondly, that row is selected where the row constant (to the right of the basic variable) has the smallest ratio to the row element in the specified column. Basic variables with a negative row element are not considered, since making one of these nonbasic would specify a point outside of the set. By this selection method, succeeding tableaux are obtained which are further and further in the direction desired.

The whole process is continued until a tableau is obtained in which all of the numbers at the bottoms of the columns under the nonbasic variables are negative. The procedure outlined has then led to the same optimum that was obtained from the graph. The value at the foot of the column just to the right of the basic variables is obtained by summing the products of the figures in the column with the corresponding figures to the left of the basic variables. This value is the total system weight for the conditions specified. This number is positive even in the final tableau. For a derivation and explanation of the process plus a discussion of certain degenerate cases, see Ref. 2. The weight is 8.9 lb, which agrees with the graphical solution shown in Fig. 1 within the accuracy of these calculations. Since the nonbasic variables in the final tableau are x_2 and x_5, this means that processes represented by these variables, H_2O_2 and KO_2, are zero.

References

[1] Charnes, A., Cooper, W. W., and Mellon, B., "Blending aviation gasolines—a study in programming interdependent activities in an integrated oil company," Econometrica **20**, 135 (April 1952).

[2] Vajda, S., *The Theory of Games and Linear Programming* (John Wiley and Sons Inc., New York, 1956).

Flutter Analysis Using Influence Matrices and Steady-State Aerodynamics

J. B. Herreshoff*
Ryan Aeronautical Company, San Diego, Calif.

MATRIX methods long used in solving vibration problems and in solving static aeroelastic problems can be combined to give solutions to the flutter problem. Steady-state aerodynamics is used, with C_{L_α} corrected by the magnitude of the Theodorsen lag function. The resulting procedure replaces the typical section approach with one using an influence coefficient description of the deflected surface and finite span aerodynamics. The flutter point is that at which two real eigenvalues merge and continue on as complex conjugates. Earlier work using steady-state aerodynamics and the mode merge criterion is discussed in Refs. 1 and 2.

The vibration problem can be solved by setting up a flexibility influence matrix, say by energy methods, converting to a dynamic matrix and iterating. The square flexibility matrix

Received August 5, 1963.
* Technical Specialist. Member AIAA.

$[F]$ relates the column matrices $\{Z\}$ and $\{P\}$, which give deflections and loads at panel points:

$$\{Z\} = [F]\{P\} \tag{1}$$

Postmultiplication of $[F]$ by the diagonal matrix of masses associated with panel points gives the dynamic matrix:

$$[D] = [F]\begin{bmatrix} \nwarrow & & \\ & M & \\ & & \searrow \end{bmatrix} \tag{2}$$

The assumption $\{Z\} = \{Z_0\}\sin\omega t$ leads to

$$\{Z\} = \omega^2[D]\{Z\} \tag{3}$$

This can be solved as an eigenvalue problem to get coupled frequencies and mode shapes.

A method of solving symmetric static aeroelastic problems can be based on the lifting surface aerodynamics described in Ref. 3. (Reference 4 can be used for the antisymmetric case.) First a matrix is constructed to relate the column matrices $\{G\}$ and $\{\theta\}$, which give circulation and twist at the control stations specified in Ref. 3:

$$\{G\} = [W]\{\theta\} \tag{4}$$

The matrix $[W]$ is the inverse of the matrix of influence coefficients given in Eq. (2) of Ref. 3. A matrix can be constructed to relate loads at panel points to circulation. This is done by panel pointing the spanwise distributions which are coefficients of G_i in Eq. (A51) of Ref. 3 for various distributions of chordwise center of pressure. The flexibility matrix gives deflections in terms of panel point loads. These steps can be compressed in matrix equations giving twist in terms of circulation and twist in terms of twist:

$$\{\theta\} = q[X]\{G\} \tag{5}$$

$$\{\theta\} = q[X][W]\{\theta\} \tag{6}$$

The dynamic pressure q enters in the conversion of circulation to loading. Now θ is the initial twist, for instance an angle of attack distribution; the elastic twist distribution θ^* is given by

$$\begin{aligned}\{\theta^*\} &= (I + q[X][W] + q^2([X][W])^2 + \ldots)\{\theta\} \\ &= (I - q[X][W])^{-1}\{\theta\}\end{aligned} \tag{7}$$

This basic equation is convenient to use in determining aeroelastic effects because of the low order of the matrices involved. For use in flutter analysis, a different form of Eq. (6) is required.

$$\{Z\} = q[A]\{Z\} \tag{8}$$

The order of $[A]$ is the same as the order of $[D]$ in Eq. (3) and the deflections are given at the same panel points. Equations (6) or (8) can be solved as an eigenvalue problem for divergence speed and mode shape.

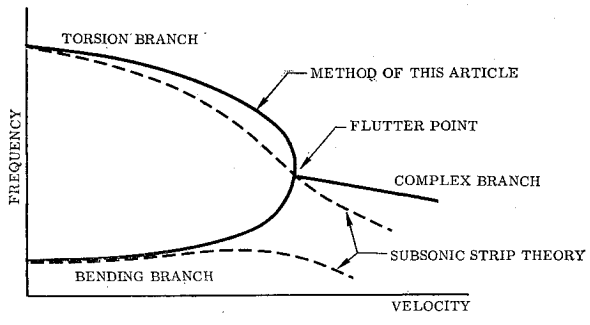

Fig. 1 Velocity-frequency curves obtained by the method of this article on Goland's wing. Subsonic strip theory results shown for comparison.

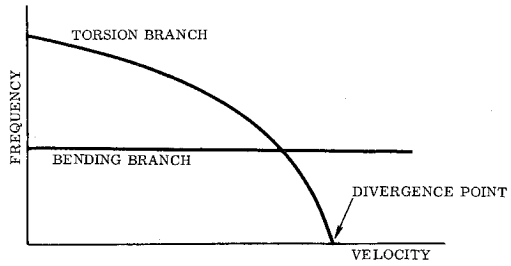

Fig. 2 Velocity-frequency curves obtained for a wing similar to Goland's but with zero static unbalance. Eigenvalues remain real and flutter is not indicated.

Combining Eqs. (3) and (8) gives

$$\{Z\} = (\omega^2[D] + q[A])\{Z\} \tag{9}$$

This eigenvalue problem can be solved in various ways to obtain a map of the frequency-velocity plane. Equation (9) is equivalent to the determinantal equations:

$$|\omega^2/q[D] + [A] - 1/q[I]| = 0 \tag{10}$$

$$|(I - \omega^2[D])^{-1}[A] - 1/q[I]| = 0 \tag{11}$$

$$|(I - q[A])^{-1}[D] - 1/\omega^2[I]| = 0 \tag{12}$$

These can be solved by iterative methods for assumed values of ω^2/q (related to reduced frequency), ω^2, or q, respectively. If the dominant root is complex, it can be evaluated using the method of Ref. 5. (In this case, the assumption $\{Z\} = \{Z_0\}e^{\lambda t}$ leads to determinantal equations with a positive sign for the coefficient of $[I]$.) The complex values of λ gave damped sinusoids, one diverging, the other converging.

The method was checked using data for the uniform wing described by Goland in Ref. 6. The mass was distributed equally to eight panel points located at the intersection of assumed front and rear spars with odd eighth points of the span. A flexibility matrix was constructed using the described stiffness properties. The eight by eight eigenvalue problem was solved by the methods just described and the results corrected by dividing the dynamic pressure by the magnitude of the Theodorsen lag function. (This correction is discussed in Ref. 1 where it is attributed to Pines.) The results of this method and of the usual subsonic strip theory flutter analysis are shown in Fig. 1. Both methods predict flutter at 335 knots and 10.5 cps. Goland's Rayleigh-Ritz method gave 334 knots and 10.73 cps, whereas his "exact" method gave 341 knots and 10.54 cps.

A further study using this method was made for a wing similar to Goland's but with no static unbalance. This showed that the bending branch was unaffected by speed, whereas the torsion branch decreased in frequency, crossed the bending branch, and ended at the divergence point. Since both branches remain real after crossing, flutter is not indicated. This result is shown in Fig. 2. Studies of this sort may be helpful to designers interested in synthesis of flutter-free structures.

This method has been used to predict flutter due to merging higher modes. Extension to wings with control surfaces would seem to present no difficulty. Structural sweep effects can be included without assuming that the wing root is perpendicular to an elastic axis. Mach number effects can be included in $[A]$ and temperature effects in $[F]$, which affects both $[A]$ and $[D]$.

Further theoretical and experimental work will be required before it is known how much confidence can be placed in the results this method gives for structures more complicated than Goland's. It has the advantage of simplicity and clarity, is almost free of Bessel functions, and stays mainly in the domain of real numbers. It has additional appeal to the structures man who has an inborn or developed distrust of elastic axes and strip theory aerodynamics.

References

[1] Zimmerman, N. H., "Elementary static aerodynamics adds significance and scope in flutter analysis," Symposium Proc. High Speed Flight, ONR-ACR-62, Vol. 1, Los Angeles, Calif. (April 1961).

[2] Bisplinghoff, R. L. and Ashley, H., *Principles of Aeroelasticity* (John Wiley and Sons, New York, 1962), pp. 269–270.

[3] De Young, J. and Harper, C. W., "Theoretical symmetric span loading at subsonic speeds for wings having arbitrary plan form," NACA TR 921 (1948).

[4] De Young, J., "Theoretical antisymmetric span loading for wings of arbitrary plane form at subsonic speeds," NACA TR 1056 (1951).

[5] Bodewig, E., *Matrix Calculus* (Interscience Publishers, New York, 1959), 2nd ed., pp. 285–289.

[6] Goland, M., "The flutter of a uniform cantilever wing," J. Appl. Mech. 12A, 197 (1945.).

Elastic Stability of Near-Perfect Shallow Spherical Shells

M. A. KRENZKE* AND T. J. KIERNAN†

David Taylor Model Basin, U. S. Navy, Washington, D. C.

Seventeen accurately machined spherical segments were collapsed under external hydrostatic pressure to determine the elastic buckling strength of near-perfect shallow spherical shells with clamped edges. Whereas previous experiments of less perfect shells recorded in the literature showed a complete lack of repeatability, the present tests follow a very definite pattern. Therefore, these tests demonstrate the critical effect of initial imperfections on collapse strength. The theories for symmetric buckling developed by Budiansky, Weinitschke, and Thurston, when combined with the theory for nonsymmetric buckling recently developed by Huang, may be used to adequately predict the behavior of the shells tested. Thus, for the first time there is good agreement between experiment and theory throughout the range of shallow spherical shells.

THE nonlinear theory for the elastic buckling strength of near-perfect shallow spherical segments with clamped edges under external hydrostatic pressure was first investigated by Feodosiev[1] in 1946. Since that time, the problem has received considerable attention. Solutions for the elastic axisymmetric buckling of initially perfect shallow spherical segments independently developed by Budiansky,[2] Weinitschke,[3] and Thurston[4] agree well with each other, but do not agree well with existing experimental data.[5–8] This disagreement is normally attributed to the fact that their theories neglected the presence of initial imperfections in the test specimens (which were formed from flat plate) and the influence of the nonsymmetric buckling mode. Both Chen[9] and Budiansky[2] have shown that the presence of initial imperfections lowers the theoretical elastic axisymmetric buckling pressure of shallow segments. However, the reduction in buckling pressure calculated for measured initial imperfections is not nearly enough to produce even fair agreement with the experimental data.[2]

Weinitschke[10] developed a theory for the nonsymmetric buckling of spherical segments which is in fair agreement with the experimental data existing prior to these present tests. Concurrent with the conduct of the present series of tests, Huang[11] developed a nonsymmetric buckling theory which was not supported by the earlier data.

Received July 27, 1963; revision received October 7, 1963.

* Head, Advanced Structures Section.

† Structural Research Engineer.

The present series of tests of machined spherical segments with clamped edges was designed to investigate the collapse strength of shells which more closely fulfill the assumptions of existing theory than was accomplished by previous experiments.

Description of Models

Seventeen shallow spherical segments with clamped edges, designated Models SS-57 through SS-73, were machined from 7075-T6 aluminum bar stock with a nominal yield strength of 80,000 psi. Young's modulus E, as determined by optical strain gage measurements, was 10.8×10^6 psi. A Poisson's ratio ν of 0.3 was assumed. The model dimensions are given in Table 1.

Departures from sphericity, variations in thickness, and residual stresses were minimized by careful selection and conduct of the machining processes. The measured variation in local inside radii for each model was less than 0.0002 in. and normally less than 0.0001 in. The measured variations in shell thickness, which are shown in Table 1, were normally less than 1% of the shell thickness. The geometric stability of the models during the final machining processes demonstrates that negligible residual stresses were present in the models after machining.

Test Procedure and Results

Each model was tested under external hydrostatic pressure. Pressure was applied in increments, and each new pressure level was held at least 1 min. The final pressure increment was less than 1% of the collapse pressure for each model. An effort was made to minimize any pressure surge when applying load.

Experimental collapse pressures are given in Table 1. Some of the models collapsed in a nonsymmetric mode, and others apparently collapsed in a symmetric mode.

Discussion

The collapse pressures of these models are compared in Fig. 1 with test results recorded in the literature and with nonlinear symmetric and nonsymmetric theory. The ordinate is the ratio of the experimental collapse pressure p_{exp} to the classical small deflection buckling pressure p_1 as developed by Zoelly and presented by Timoshenko.[11] The abscissa is the nondimensional geometric parameter θ defined as

$$\theta = \left[\frac{3}{4}(1-\nu^2)\right]^{1/4} \frac{C}{(Rh)^{1/2}} = \frac{0.91C}{(Rh)^{1/2}} \text{ for } \nu = 0.3 \quad (1)$$

where R is the radius to the midsurface of the shell, h is the

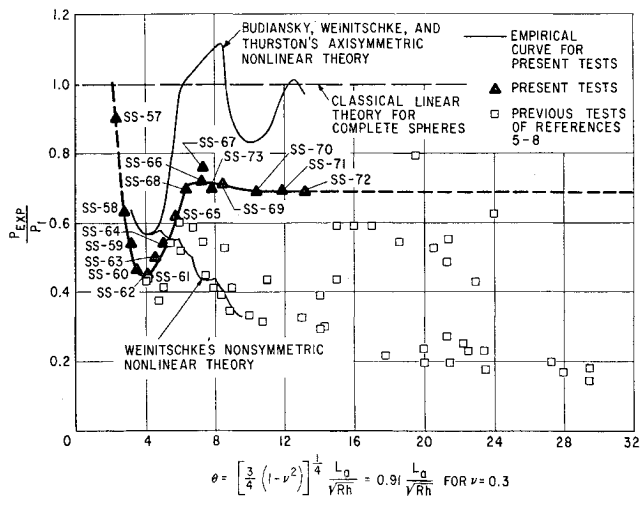

Fig. 1. Experimental elastic buckling data for shallow spherical shells with clamped edges.